Journal of the European Ceramic Society 22 (2002) 851–862

www.elsevier.com/locate/jeurceramsoc

# Stabilized nanoparticles of metastable $ZrO_2$ with $Cr^{3+}/Cr^{4+}$ cations: preparation from a polymer precursor and the study of the thermal and structural properties

J.C. Ray, C.R. Saha, P. Pramanik*

*Department of Chemistry, Indian Institute of Technology, Kharagpur 721 302, West Bengal, India*

Received 2 May 2001; accepted 10 July 2001

**Abstract**

Nanoparticles of stabilized $ZrO_2$ in a single cubic phase by 5–20 at.% (of total metal cations) $Cr^{3+}/Cr^{4+}$ addition are obtained through a chemical method using a polymer matrix made of sucrose and polyvinyl alcohol. On heating at 250–900 °C in air, the polymer network decomposes and burns out leaving behind a dispersed microstructure in 10–25 nm diameter particles of cubic $ZrO_2$ in spherical shape. A modified microstructure comprises of 10–14 nm crystallites of dispersed tetragonal phase, or both tetragonal and monoclinic phases, in cubic phase appear on a prolong (2 h or larger) heating of precursor at 900–950 °C. Particles in tetragonal $ZrO_2$ are in acicular shape, while the monoclinic phase is in the shape of platelets. The $Cr^{3+}/Cr^{4+}$ additive facilitates formation of cubic phase in small particles on a controlled decomposition and combustion of precursor. It stabilizes small particles by inhibiting their growth by forming a thin amorphous surface layer over them. 

*Keywords:* Cr-stabilised $ZrO_2$; Nanoparticles; Powders-chemical preparation; Precursors-organic; $ZrO_2$

## 1. Introduction

The polymorphism of $ZrO_2$ is very well known.[1–3] The different $ZrO_2$ phases have their own intrinsic physical and chemical properties, which make them as one of the most important engineering ceramic materials. High hardness, low wear resistance, low coefficient of friction, high elastic modulus, chemical inertness, good ionic conductivity, low thermal conductivity, and high melting temperature are their common properties.[2,4] A displacive t→m phase transformation,[1,2] limits applications of m-$ZrO_2$ as refractory or other engineering materials. It invokes a catastrophic fracture.[2] It can be resolved if replacing m-phase by other phases. Efforts are being made to stabilize them on controlled crystallite size at a nanometer scale with dopants of MgO, CaO, $Y_2O_3$, $CeO_2$, $Mg_3N_2$, $Si_3N_4$, AlN, etc.[1–8] Hydrothermal process,[7] vapor phase hydrolysis,[8] spray pyrolysis,[9] gas condensation,[10] sol-gel process,[11] and combustion methods[12] have been explored in order to have a controlled microstructure.

As such, $Cr^{3+}$ is hardly soluble in $ZrO_2$ and this amount is insufficient to stabilize c- and t-phases by conventional methods.[13–16] $ZrO_2$ admixed with $Cr_2O_3$ has applications of catalytic uses, in production of $H_2$ by $H_2O$ dissociation, as a potential conductor in magneto-hydrodynamic generators,[13,15] and in producing $H_2$ and carboxylic acids from water vapor and aldehyde, in decomposition of $CHC1F_2$, in production of green chromophores.[16] Stabilized c-$ZrO_2$ is specially used as oxygen sensor,[11] solid fuel cells,[17] and ceramic components[14] and as catalyst or catalyst promoter in synthesizing alcohol by hydrogenation of CO.[15] It has plenty of oxygen vacancies to act as active sites in catalytic activity.[18] A partially stabilized or a multiphase $ZrO_2$ forms transformation-toughened composites.[1,2] A fine-scale precipitate of m-$ZrO_2$ and/or t-$ZrO_2$ in a stabilized c-$ZrO_2$ matrix improves toughness.[19] It gives a new strengthening mechanism in composites by a strong macroscopic interaction between components.[2,19]

In this article, we report synthesis of $Cr^{3+}/Cr^{4+}$ stabilized c-$ZrO_2$ nanocrystals through a new chemical method[20–22] using metal cations in a solution of sucrose

* Corresponding author. Fax: +91-3222-55303.
*E-mail address:* pramanik@chem.iitkgp.ernet.in (P. Pramanik).

0955-2219/02/$ - see front matter 
PII: S0955-2219(01)00404-6

and polyvinyl alcohol (PVA). Stabilized c-$ZrO_2$ appears on decomposition of precursor at 900 °C or lower temperature. A modified microstructure with dispersed t- and/or m-phase(s) in c-$ZrO_2$ develops at subsequently higher temperatures. Stable c-$ZrO_2$ forms and exists in small particles in a distorted lattice in support of the $Cr^{3+}/Cr^{4+}$ additives.

## 2. Experimental

### 2.1. Synthesis

A polymer precursor with dispersed $Zr^{4+}$ and $Cr^{3+}/Cr^{4+}$ cations in a specific ratio is obtained by reaction of analytical grade (i), $Zr(OH)_4{\cdot}xH_2O$ (ii) $(NH_4)_2Cr_2O_7$, (iii) sucrose, and (iv) PVA. White gelatinous precipitate of $Zr(OH)_4{\cdot}xH_2O$ is obtained by the reaction of $ZrOCl_2{\cdot}8H_2O$ and $NH_4OH$ in aqueous solution. $Zr(OH)_4{\cdot}xH_2O$ is dissolved in nitric acid to form solution of $ZrO(NO_3)_2$ and $Cr^{6+}$ cations are added through an aqueous $(NH_4)_2Cr_2O_7$ solution in a molar concentration. Addition of sucrose and PVA (mol wt. 125,000) by 50–70% in a batch of 20 g sample yields a final precursor solution in a transparent light green color. A molar ratio in sucrose and PVA monomer is about 10:1.

The solution is dried over a water bath into a precursor mass of a dark black color. The latter is pyrolyzed into a fluffy powder having light brown to deep blue color as per $C_{Cr}$ (atomic percent of chromium cations) content on a hot plate at ~250 °C. Calcinations at 600–900 °C results in a stabilized $ZrO_2$ nanopowder. A series of samples with $C_{Cr}$ content up to 30 at.% have thus been obtained after calcining at representative temperatures.

### 2.2. Characterization and measurements

Thermal decomposition/combustion of precursor mass to $ZrO_2$ is studied with thermogravimetric analysis (TG) and differential thermal analysis (DTA) using a thermal analyzer (Model DT-40, Shimadzu Co., Kyoto, Japan). The data are collected by heating the sample at 5 °C/min. Phase analysis is carried out with X-ray diffraction of representative samples with the help of a Philips PW-1804 X-ray powder diffractometer with Ni filtered Cu$K_\alpha$ radiation of wavelength $\lambda = 0.15418$ nm. Average crystallite size '$d$' is calculated from width $\Delta 2\theta_{1/2}$ in characteristic peaks with the Debye Scherrer formula.[23] Size and morphology of particles in powder are studied with a transmission electron microscope (TEM) of Hitachi H-600. Chemical compositions of samples are confirmed by in situ EDX analysis with SEM micrographs of Hitachi S-415A. The sample in TEM analysis was prepared by dispersing powder in alcohol over an ultrasonic bath. A drop of suspension was carefully placed with a syringe on a carbon coated Formvar film predeposited on a copper grid, which was ultimately loaded with sample in the microscope for the analysis. The presence of $Cr^{3+}$ and $Cr^{4+}$ are analyzed in powders by chemical test and by measuring paramagnetic moment by Gouy Balance (Model No. Dhona 100 DS).

## 3. Results and discussion

### 3.1. Reaction process in formation of polymer precursor

The formation of a polymer precursor with metal cations in an aqueous sucrose-PVA solution and its decomposition to $ZrO_2$ nanopowder are shown as follows:

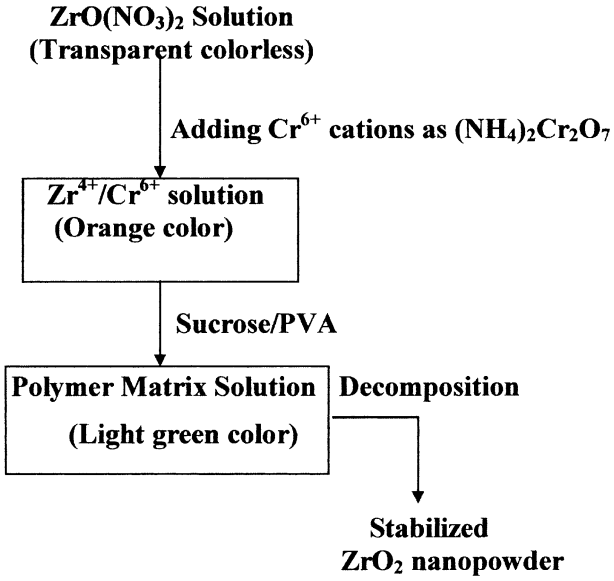


Sucrose and PVA forms a polymer with dissolved metal cations in water. Here, sucrose plays a multifunctional role. At first, it forms a complex with metal cations by coordinating through hydroxyl groups. It circumvents selective precipitation of coordinating cations while evaporating the excess water in the solution to a dried precursor mass.

### 3.2. Reconstructive decomposition and combustion in precursor

In order to get refined $ZrO_2$ particles in controlled size in few nanometers, the precursor mass is first heated over a hot plate at low temperature as ~250 °C. This temperature is insufficient to induce its spontaneous combustion. The dried mass slowly decomposes into carbonaceous residue, which is mesoporous carbon imbedded with oxide particles. The carbonaceous mass is slowly oxidizes in presence of air due to catalytic activity of $Cr^{3+}/Cr^{4+}$ below its ignition temperature. It helps to generate the controlled phase of $ZrO_2$ containing $Cr^{3+}/Cr^{4+}$ ions.

Fig. 1 shows DTA and TG curves in thermal decomposition/combustion during heating 6.4 mg of a precursor

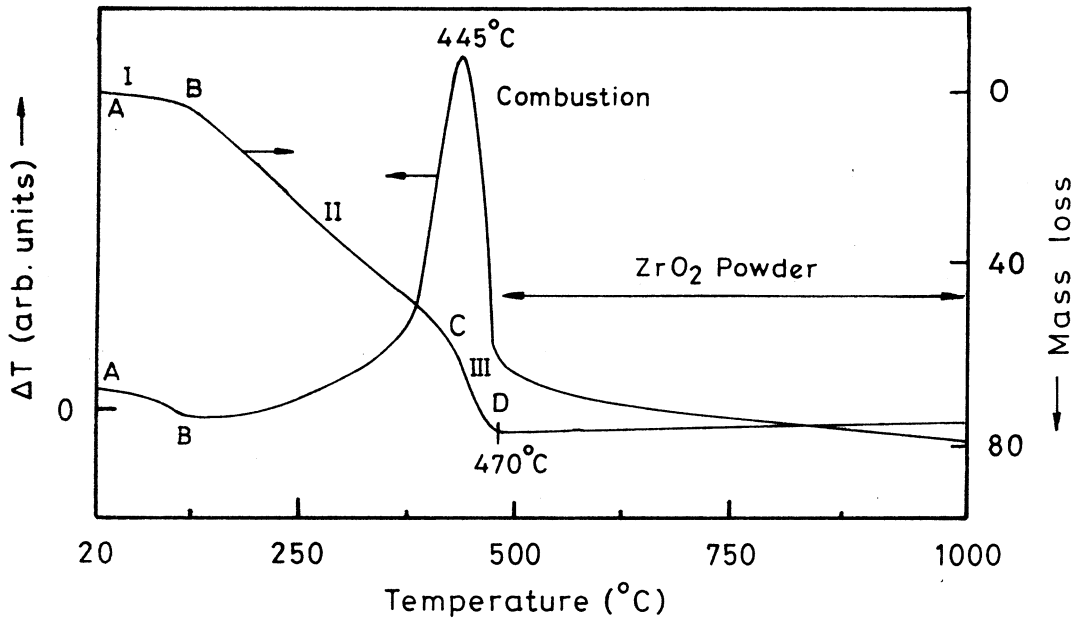


Fig. 1. DTA and TG thermograms in a polymer precursor ($C_{Cr}=10$ at.% and dried over a water bath) during heating at 5 °C/min.

(containing 10 at.% $C_{Cr}$ and dried at 100 °C over a water bath) at 5 °C/min. A decomposition with a predominant combustion by an exothermic peak in combustion occurs at $T_{PC}=445$ °C with a total $\Delta M=78$ mass loss. The mass loss in TG curve occurs in three (I, II and III) successive steps among points of A, B, C and D. Signal I, which involves $\Delta M\sim3\%$ and lasts to ~150 °C, indicates desorption of part of $H_2O$ and interstitial gases if any. Generation and incorporation of CO, $CO_2$ and $NH_3$ gases in the sample are common during its processing. Signal II has $\Delta M\sim50\%$ and extends to 430 °C while signal III, $\Delta M\sim25\%$, lasts at point D at $T_{CC}\sim470$ °C (complete combustion temperature). No further loss in mass appears over higher temperatures.

In principle, a desorption or decomposition is an endothermic process. It involves absorption of heat by excitation of the system through a series of energy levels to the limit of its thermodynamic stability from which it ultimately occurs. This is very much reflected in by desorption of $H_2O$ and interstitial gases in signal I between points A and B (Fig. 1). Also, decomposition at early temperatures in signal II begins with an altogether endothermic heat output. Monotonically increasing rate of heat output leads to spontaneous combustion of sample in prominent exothermic signal III at subsequent temperatures.

As portrayed in Figs. 2 and 3, the values in both $T_{PC}$and $T_{CC}$are decreasing with increasing $C_{Cr}$. Extrapolations of two curves to $C_{Cr}\rightarrow0$ yield their maximal values of $T^m_{PC}=464$°C and $T^m_{CC}=662$ °C, which are as large as 51% of those of 390 and 437 °C, respectively, at $C_{Cr}\sim30$ at.%. In a similar inorganic precursor in hydrazine $(NH_2)_2{\cdot}H_2O$,[15] the $Cr^{3+}$ enhances its temperature of recrystallization $T_C$ into $ZrO_2$ nanoparticles. A rather large $T_C=477$ °C value (which can be treated as our $T^m_{PC}$ value) appears at 5 at.% $C_{Cr}$ and it shifts further as 615 and 713 °C at 20 and 30 at.% $C_{Cr}$.[15]

A simulation to the experimental data points with a straight line,

$$T_{PC}=\alpha C_{Cr}+\beta \tag{1}$$

reproduces the result (shown by the line in Fig. 2) with $\alpha=-4.9$ °C/mol and $\beta=464$ °C, i.e. the value of $T_{PC}$at $C_{Cr}=0$. An empirical exponential function,

$$T_{CC}=\gamma T^m_{CC}\exp-\left[\frac{C_{Cr}}{C_{Zr}}\right]^n \tag{2}$$

describes the $T_{CC}$ vs $C_{Cr}$ plot shown by the solid curve in Fig. 3. A best fit to the data appears assuming an empirical value 0.95 for the correlation constant $\gamma$ with an exponent $n=0.5$. These model variations of $T_{CC}$ and $T_{PC}$ with $C_{Cr}$ demonstrate the fact that $C_{Cr}$ imparts structure of precursor and in turn influence kinetics of (i) its combustion process and (ii) formation of stabilized $ZrO_2$ by reaction of its decomposed species of metal cations during combustion. The $Cr^{3+}/Cr^{4+}$ cations behave as an internal catalyst to facilitate the combustion at moderate temperature. This is the reason that they function as a stabilizing agent in forming stabilized $ZrO_2$ in small particles at moderate temperature insufficient to induce their growth further by recombination reaction.

### 3.3. Phase analysis

X-ray diffraction (Fig. 4) with two halos at wavevectors $q_1=8.9$ and $q_2\sim30.0$ nm$^{-1}$ (defined by $q=4\pi\sin\theta/\lambda$)

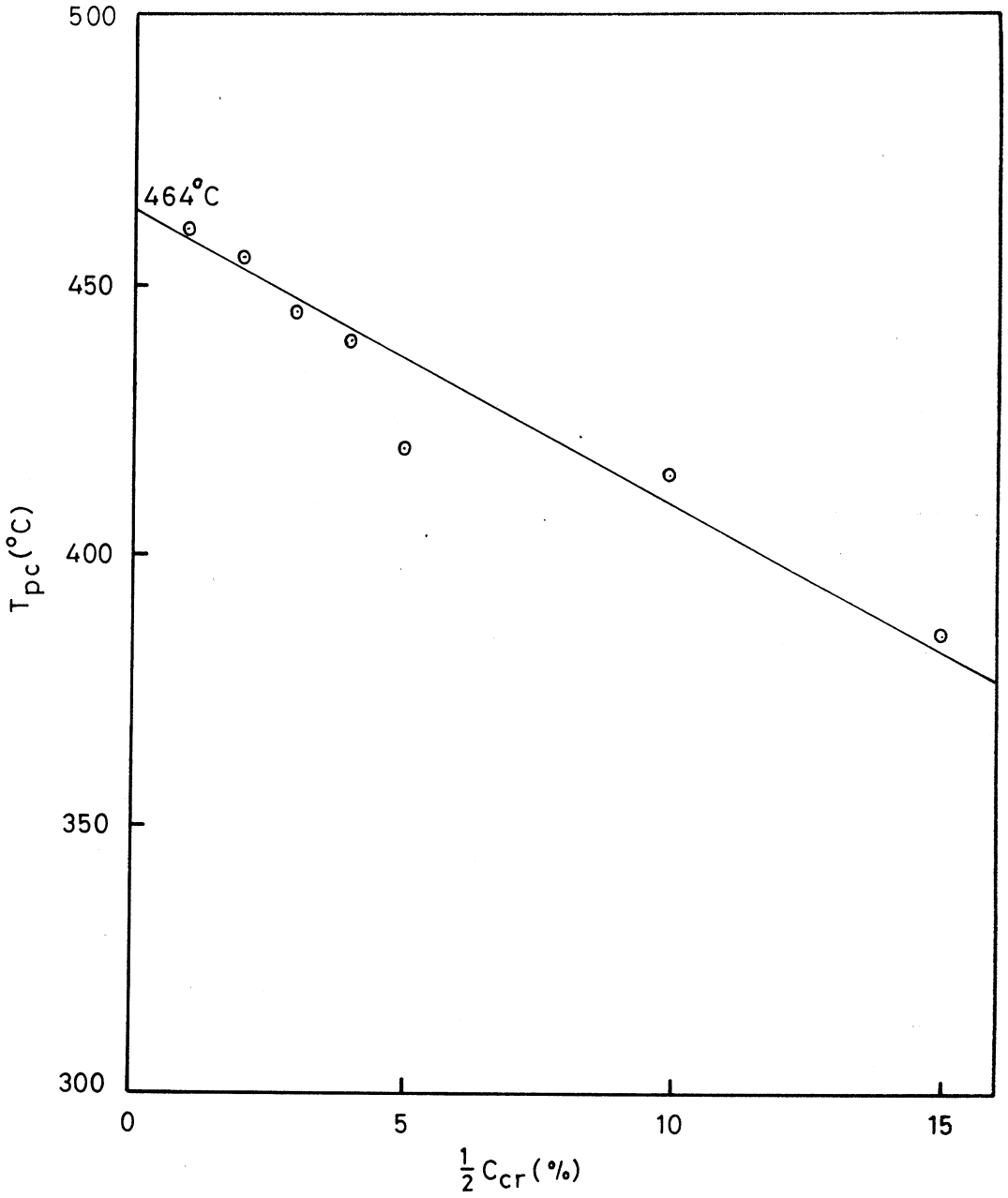


Fig. 2. A plot of exothermic peak temperature $T_{PC}$ in DTA curve with a function of $C_{Cr}$ in polymer precursor.

characterizes amorphous structure of precursor powder dried over a water bath with 10 or 20 at.% $C_{Cr}$. Their average positions have a marginal shift, as much as 2.4 $nm^{-1}$, in comparison to those in PVA or PVA-sucrose polymer. This is expected in predominant local structure of polymer component. In addition to two $q_1 = 11.3$ and $q_2 \sim 28.6$ $nm^{-1}$ halos in amorphous structure, the polymer has four sharp peaks at 0.394, 0.444, 0.528 and 0.633 nm in part of a nanocrystalline component of it. It gets dissolved in amorphous structure on adding metal cations to synthesize the metal-organic complex precursor.

A recrystallization from amorphous precursor results in stabilized $ZrO_2$ nanoparticles above 250 °C. For example, Fig. 5 compares X-ray diffraction of stabilized $ZrO_2$ with $C_{Cr} = 10$ at.% by calcining the precursor at (a) 250, (b) 800, (c) 900 and (d) 950 °C for 4 or 2 h. A pure c-$ZrO_2$ phase forms at 250 °C in (a) and stable up to 800 °C in (b). Part of it converts into t-$ZrO_2$ on raising the temperature to 900 °C in (c), resulting in dispersed t-$ZrO_2$ nanoparticles in the matrix of c-$ZrO_2$ in a stable equilibrium at or below 900 °C. No $Cr^{3+}$ cations segregate in an independent crystalline phase, confirming their solubility in c- or t-$ZrO_2$ nanoparticles.

A phase separation of $Cr^{3+}$ as $Cr_2O_3$ having hexagonal crystal structure $(h)$[24a] together with formation of m-$ZrO_2$ from c-$ZrO_2$ occurs above and at the temperature 950 °C

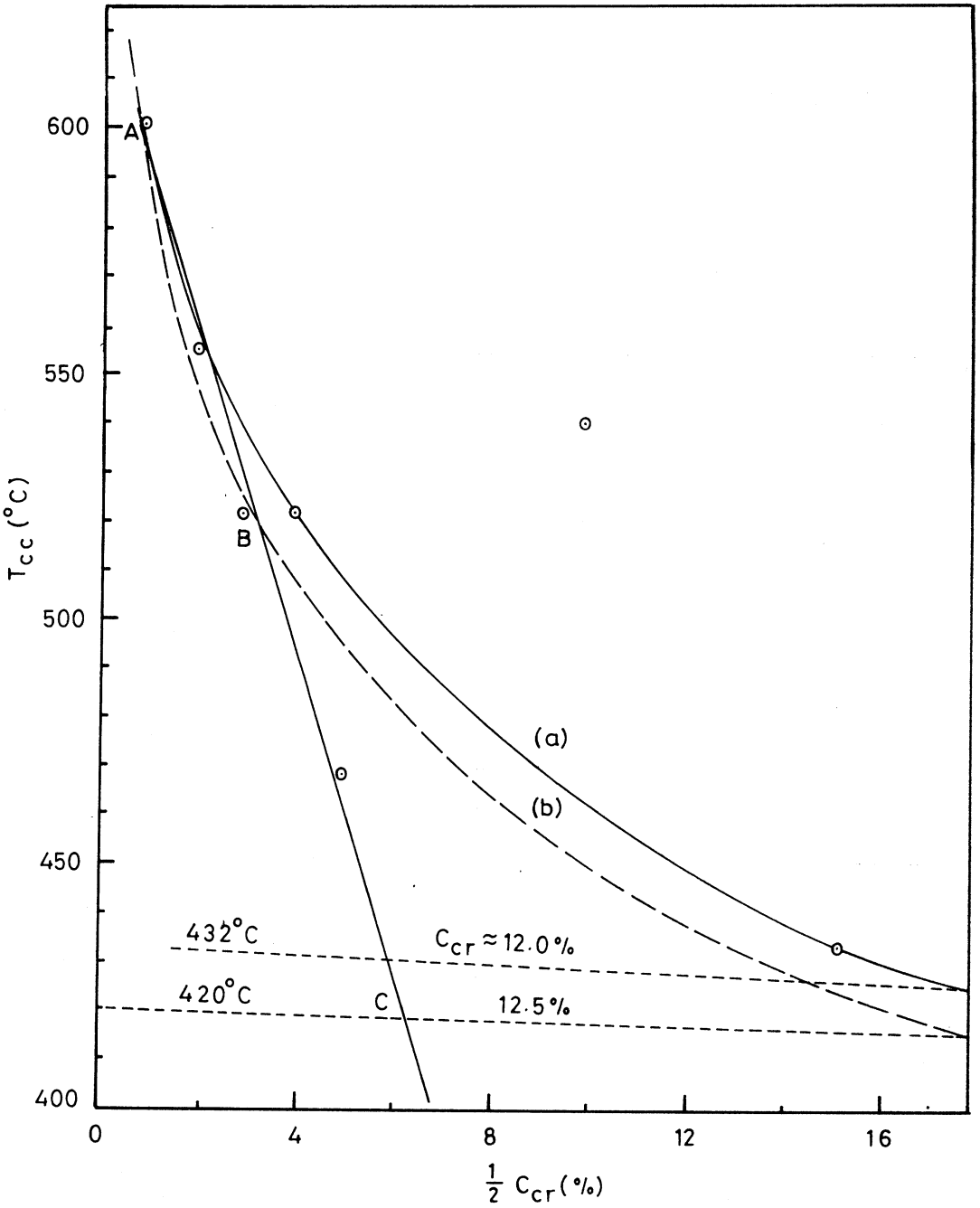


Fig. 3. A plot of complete combustion (constant weight) temperature $T_{CC}$ in TG with a function of $C_{Cr}$ in polymer precursor, (a) experimental and (b) simulation. A linear plot over early data points of ABC intersects their tangents at (a) $C_{Cr} = 12.0$ and (b) 12.5%.

[Fig. 5(d)] or by a prolonged heating at 900 °C for 15 h. The result envisages that c-$ZrO_2$ crystallizes from amorphous state in a solid solution with $Cr^{3+}/Cr^{4+}$ cations. Its capacity to dissolve $Cr^{3+}/Cr^{4+}$ in it varies with its size of crystallites. Small crystallites generated at effectively low temperature have a significant solubility of $Cr^{3+}/Cr^{4+}$. This is due to more defects in the smaller crystallites of c-$ZrO_2$ produced at relatively lower temperature. The reactions can be expressed as follows:

$$\text{Amorphous precursor} \xrightarrow{\text{Above } 250^\circ\text{C}} \text{c-}ZrO_2\ (\text{ss}) \xrightarrow{900^\circ\text{C}}$$

$$\text{c-}ZrO_2\ (\text{ss}) + \text{t-}ZrO_2(\text{ss}) \xrightarrow{950^\circ\text{C}} \text{c-}ZrO_2\ (\text{ss})$$

$$+ \text{t-}ZrO_2(\text{ss}) + \text{m-}ZrO_2(\text{ss}) + \text{h-}Cr_2O_3 \xrightarrow{1050^\circ\text{C}}$$

$$\text{m-}ZrO_2(\text{ss}) + \text{h-}Cr_2O_3$$

A phase transformation of t-$ZrO_2$ (ss) into m-$ZrO_2$(ss) occurs on prolonged heating at 900 °C or above. Raising the temperature above 900 °C has similar results with a

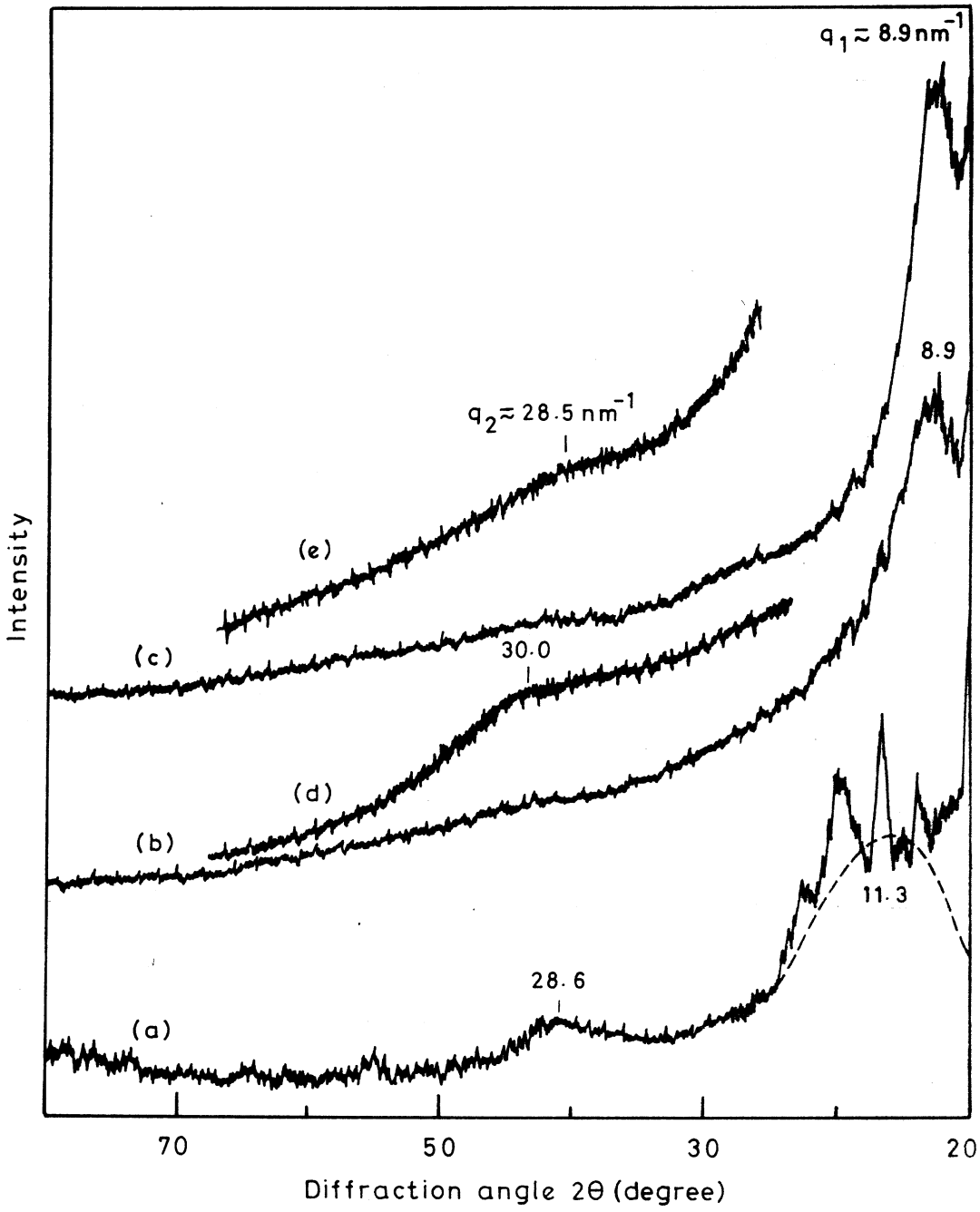


Fig. 4. X-ray diffraction in (a) PVA and polymer precursor with (b) 10 and (c) 20% $C_{Cr}$. A prominent halo $q_1$ appears at wave vector (a) 11.3 and (b) 8.9 and (c) 8.9 $nm^{-1}$. Parts of diffractograms (b) and (c) at a magnified scale indicate a weak halo $q_2$ at (d) 30.0 and (e) 28.5 $nm^{-1}$ in comparison to that at (a) 28.6 $nm^{-1}$.

single m-$ZrO_2$ with incipient growth of h-$Cr_2O_3$ ($a=0.4954$ and $c=0.1358$ nm)[24a] at 1050 °C (Fig. 6). The lattice parameters of m-$ZrO_2$ are $a=0.5140$ nm, $b=0.5195$ nm, $c=0.5305$ nm, and $\beta=99°23$ min calculated by positions (interplanar spacing $d_{hkl}$) of diffraction peaks. Its change by ~0.2% if compared to $a=0.5148$ nm, $b=$ 0.5203 nm, $c=0.5316$ nm, and $\beta=99°23'$ values[24b] of pure m-$ZrO_2$. This indicates no significant $Cr^{3+}$ solubility in m-$ZrO_2$.

A manifested reaction forming t-$ZrO_2$ (ss) at larger $C_{Cr}=20$ at.%, or even more, results in t-$ZrO_2$ (ss) with h-$Cr_2O_3$ as early as at 800 °C (Fig. 7). But similar with 10 at.% except higher separation of h-$Cr_2O_3$ on raising the temperatures further as 1050 °C (Fig. 6). A value of $C_{Cr}$ above 20 at.% is not so useful as it adds impurities of h-$Cr_2O_3$ even at low temperatures as 250 °C.

The present results differ from those of $Cr^{3+}$ stabilized $ZrO_2$ recrystallized from amorphous $ZrO_2$–$Cr_2O_3$ precursor obtained by precipitation reaction of metal chlorides with hydrazine [$(NH_2)_2 \cdot H_2O$] in water and then drying the recovered precipitate at 120 °C under

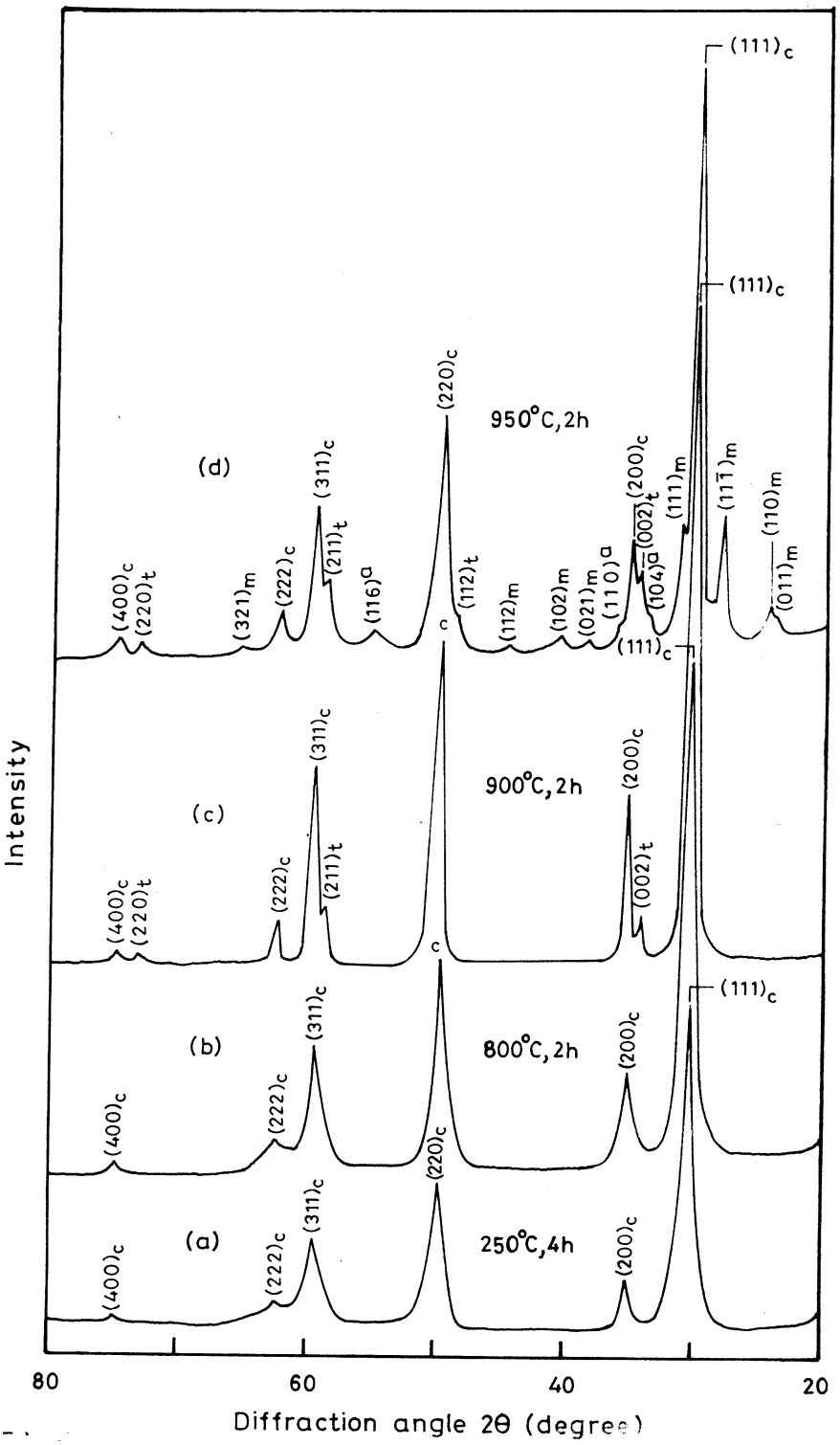


Fig. 5. X-ray diffraction in stabilized $ZrO_2$ on calcining the precursor with $C_{Cr}=10\%$ at (a) 250, (b) 800, (c) 900, and (d) 950 °C. At 900 °C or above, part of c-$ZrO_2$ in (a) or (b) transforms to (c) t-$ZrO_2$ and (d) t-$ZrO_2$ and m-$ZrO_2$. Their peaks are marked by (hkl) with subscripts c, t and m, respectively, while those in h-$Cr_2O_3$ are marked with superscript a.

reduced pressure.[15] In this case, t-$ZrO_2$ forms instead of c-$ZrO_2$ even at low 465 to 750 °C temperatures by dissolving as much $Cr_2O_3$ as 11 mol%. At higher 900 °C and above temperatures, $Cr^{3+}$ precipitates and t-$ZrO_2$ converts into m-$ZrO_2$. A mixture in c- and m-phases appears at larger $Cr_2O_3$ contents till 20 at.%. $Cr^{4+}$ cations in combination with those of $Cr^{3+}$ in this example seems responsible to stabilize a single-phase c-

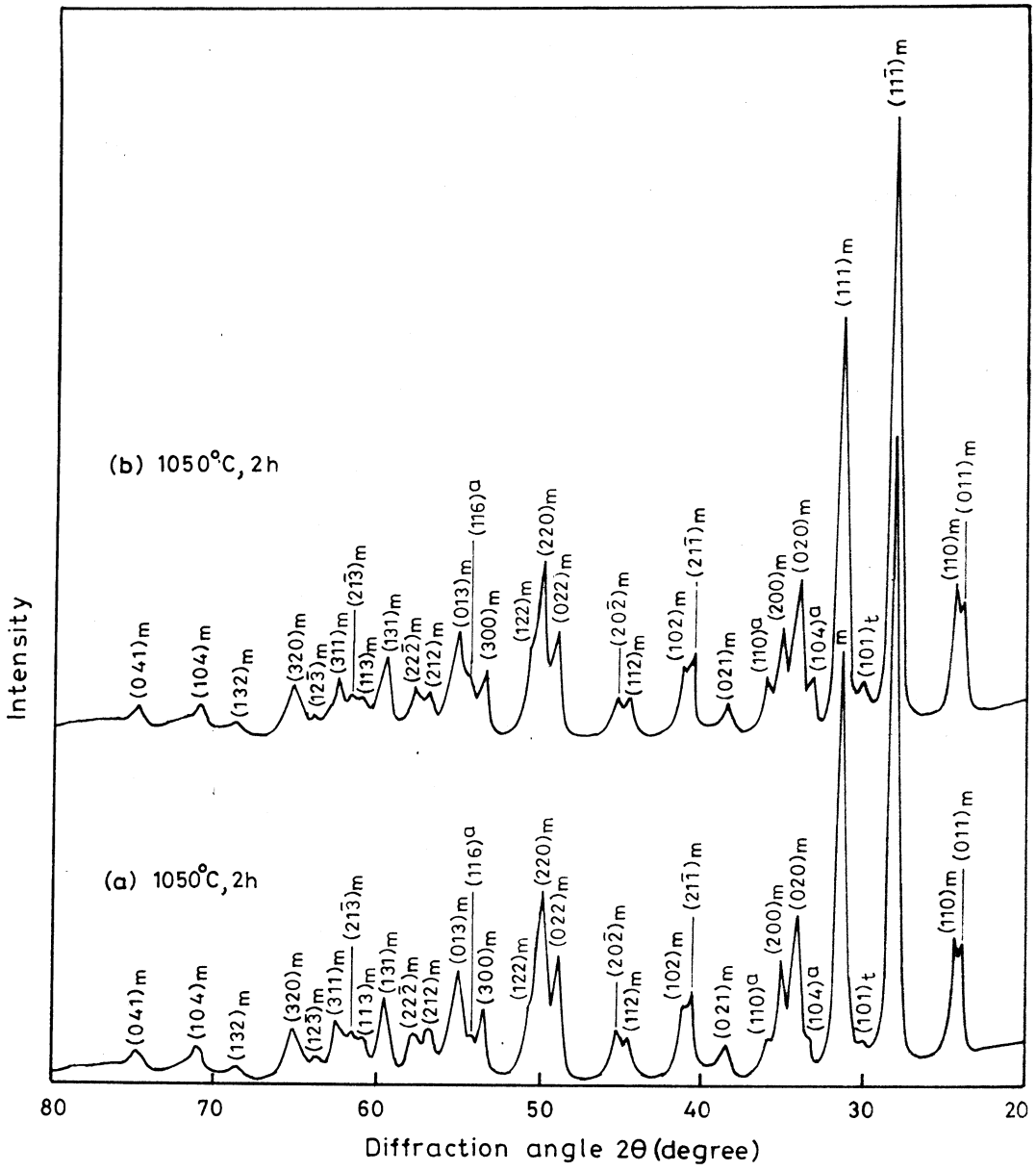


Fig. 6. X-ray diffraction in a complete phase transformation of low temperature polymorphs into m-$ZrO_2$ with a differential h-$Cr_2O_3$ separation at 1050 °C; (a) $C_{Cr}=10$ and (b) 20%.

$ZrO_2$ in controlled size in a few nanometers. As the results are summarized in Table 1, a pure c-$ZrO_2$ forms with 5–10 at.% $C_{Cr}$. As such this small $C_{Cr}$ retains improved stability of c-$ZrO_2$ nanoparticles, especially in presence of other polymorphs, to as high temperature as 950 °C.

Stabilized c-$ZrO_2$ with 2 at.% $C_{cr}$ has a larger lattice parameter $a=0.5130$ nm of undoped bulk sample ($a=0.5090$ nm).[24d] An increase in $C_{cr}$ reflects in a little decrease in its value to 0.5070 nm at $C_{cr}\sim10$ at.% as per the c-$ZrO_2$ + $C_{cr}$ $Cr^{3+}/Cr^{4+}\rightarrow$c-$ZrO_2$ (ss) solid solution formation. It accords to smaller ionic radius $r=0.062$ nm in $Cr^{3+}/Cr^{4+}$ over $r=0.084$ nm in $Zr^{4+}$. Dissolution of $Cr^{3+}/Cr^{4+}$ in t-$ZrO_2$ involves a maximum 1.0% decrease (at $C_{cr}\sim10$ at.%) in $c=0.5220$ nm and 0.28% in $a=0.3630$ nm lattice parameters against $a=0.5270$ and $c=0.3640$ nm bulk values.[24e] No change occurs in 'a' if stabilizing by $Cr^{3+}$ alone.[15] Possibly, it occupies the sites primarily along *c*-axis.

Volume fraction $V_m$ in m-$ZrO_2$ dispersed in matrix of c-$ZrO_2$ and t-$ZrO_2$ is estimated by partial integrated intensity $X_m$ in its first $(11\bar{1})$ and second (111) most intense X-ray diffractograms peaks with the $V_m = PX_m\{1+(P-1)X_m\}^{-1}$ relation.[25] Correlation constant $P=1.31$ accounts for non-linearity in $V_m$ as function of $X_m$.[25] A numerical value of $X_m$ is obtained from Eq. (3) by the areas $I_m(11\bar{1})$ and $I_m$ (111) in $(11\bar{1})$ and (111) peaks respectively in m-$ZrO_2$,

$$X_m = \frac{I_m(11\bar{1}) + I_m(111)}{I_m(11\bar{1}) + I_m(111) + I_t(101)/I_c(111)} \quad (3)$$

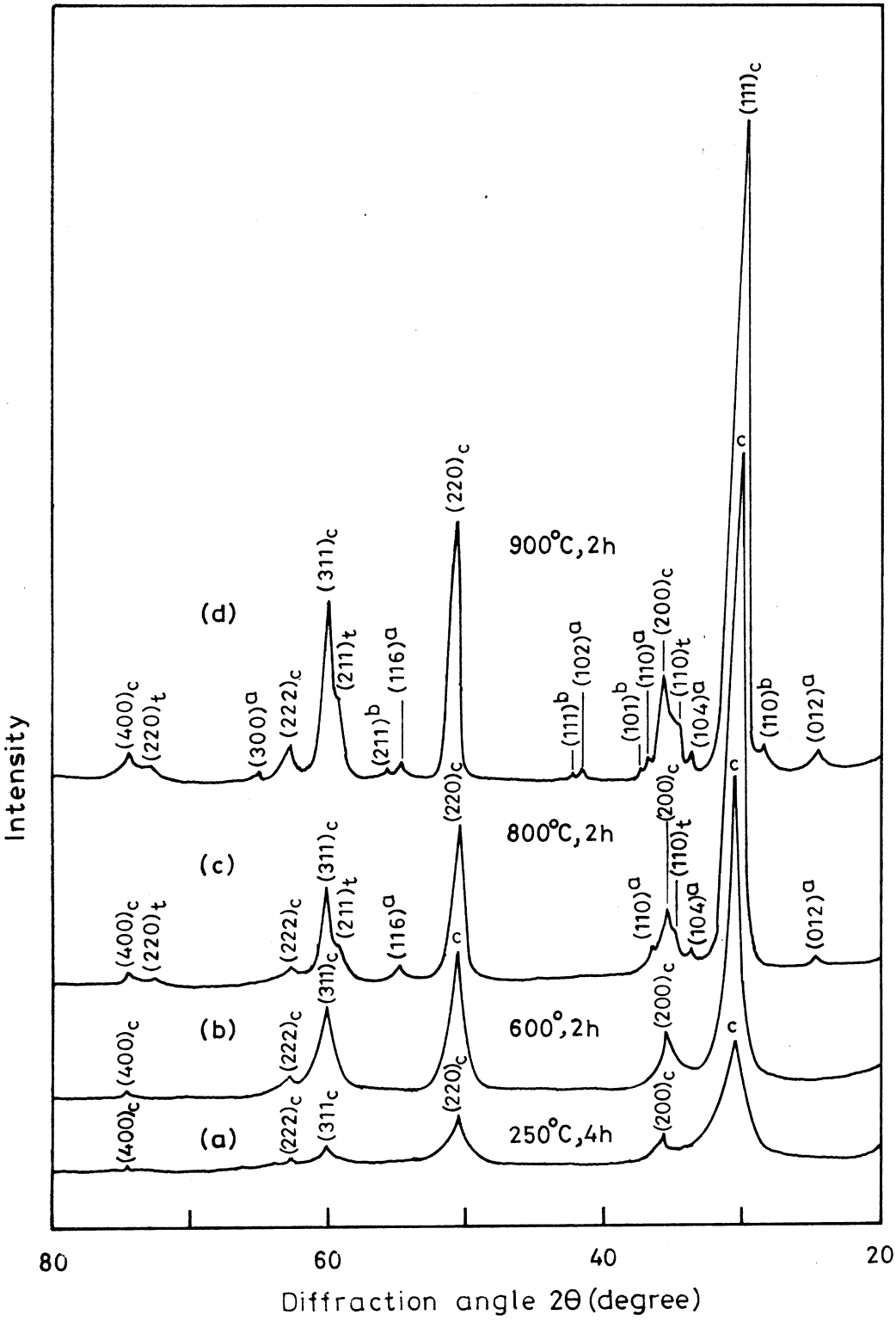


Fig. 7. X-ray diffraction in stabilized $ZrO_2$ on calcining the precursor with $C_{Cr}=20\%$ at (a) 250, (b) 600, (c) 800, and (d) 900 °C. Phase transformation from c-$ZrO_2$ to t-$ZrO_2$ starts with h-$Cr_2O_3$ segregation at moderate temperature as 800 °C. A t-$CrO_2$ phase (marked by b) appears at 900 °C.

$I_t$ (101) in the most intense (101) peak in t-$ZrO_2$, and $I_c$(111) in the most intense (111) peak in c-$ZrO_2$ satisfactorily reproduces $V_m$. For example, the powder ($C_{cr}=10$ at.% and annealed 2 h at 950 °C) in Fig. 5d, has $X_m \sim 0.3$, which determines $V_m=36\%$. As per peak intensity, $I=25\%$ (against $I=20$ standard value) in (311) peak in c-$ZrO_2$ and $I=13\%$ ($I=15$ standard value) in (211) in t-$ZrO_2$, volume $V_c$ in *c*-phase is as

Table 1
Average crystallite size $d$, surface area $\Omega$, and visible color in stabilized $ZrO_2$ nanoparticles with 10 at.% $Cr^{3+}/Cr^{4+}$ additive

| Samples | Color | Structure | $d$ (nm)[a] | $\Omega$ ($m^2/g$)[b] |
|---|---|---|---|---|
| 1. Virgin precursor | Black | Amorphous | | |
| 2. Sample 1 pyrolysed over a hot plate at 250 °C | Light yellow–brown | c-$ZrO_2$ | 5 (10–15) | 197 |
| 3. Sample 2 calcined 2 h at 600–800 °C | Light yellow–brown | c-$ZrO_2$ | 8 (10–25) | 130 |
| 4. Sample 2 calcined 2 h at 900 °C | Light yellow–blue | c and t-$ZrO_2$ | 10 (10–25) | 98 |
| 5. Sample 3 heated 15 h at 900 °C | Light blue | c, t and m-$ZrO_2$ | 14 (30–50) | 70 |
| 6. Sample 3 heated 2 h at 950 °C | Light blue | c, t and m-$ZrO_2$ | 14 (30–60) | 70 |
| 7. Sample 2 calcined 2 h at 1050 °C | Light blue | m-$ZrO_2$ | 16 (80–160) | 61 |

[a] Average $d$ value calculated from widths in X-ray diffraction peaks and the observed particle size from TEM in the parentheses. Crystallites are clustered in particles.
[b] Average $\Omega$ value obtained in approximation of spherical shape of crystallites.

much as 1.5 times in t-phase. The values obtained for other powders are included in Table 2.

### 3.4. Size and morphology in $ZrO_2$ particles

Stabilized c-$ZrO_2$ particles or crystallites are in spherical shape in TEM micrograph. Their morphology as well as size does not change much by recrystallization from precursor between 250 and 800 °C. For example, TEM micrographs from a recrystallized precursor, $C_{Cr} = 10$ at.%, at (a) 250 °C and (b) 800 °C are compared in Fig. 8. Average particle diameter, $D$, hardly changes from 12 nm in (a) to 20 nm in (b). A modified acicular morphology appears in t-$ZrO_2$ in Fig. 9(a) on raising the temperature at 900 °C. The particles are as long as 600 nm in 10–40 nm widths with aspect ratio $\phi \leqslant 15$. As shown in Fig. 9(b) from a selected region, part of particles, which are still in c-$ZrO_2$ phase, have an oval shape in $D = 35$ nm in growth process to t-$ZrO_2$.

### 3.5. Chemical analysis of the presence of $Cr^{4+}$ and $Cr^{3+}$

The chemical analysis of the samples are done as follows by iodometric method. Qualitative analysis: 0.1 g of K*I* followed by 5.0 ml of $CH_3COOH$ is added to a suspension of an 0.2-g sample in 20 ml of distilled water. A reaction of $Cr^{4+}$ occurs with K*I* by releasing $I_2$ gas according to the following reaction:

Table 2
Chemical compositions and experimental conditions of recrystallization of $Cr^{3+}/Cr^{4+}$ stabilized $ZrO_2$ from polymer precursors in different polymorphs

| $C_{Cr}$ (at.%) | Annealing | | $ZrO_2$ polymorphs[a] |
|---|---|---|---|
| | Temperature (°C) | Time (h) | |
| 4 | 250–800 | 2–4 | c-$ZrO_2$, t-$ZrO_2$ (25), m-$ZrO_2$ (10) |
| 10 | 250–800 | 2–4 | c-$ZrO_2$ |
| | 900 | 2 | c-$ZrO_2$, t-$ZrO_2$ (25) |
| | 900 | 15 | c-$ZrO_2$, t-$ZrO_2$ (30), m-$ZrO_2$ (20), h-$Cr_2O_3$ |
| | 950 | 2 | c-$ZrO_2$, t-$ZrO_2$ (25), m-$ZrO_2$ (35), h-$CrO_2$ |
| | 1050 | 2 | m-$ZrO_2$, h-$Cr_2O_3$ |
| 20 | 250–600 | 2–4 | c-$ZrO_2$ |
| | 800 | 2 | c-$ZrO_2$, t-$ZrO_2$ (35), h-$Cr_2O_3$ |
| | 900 | 2 | c-$ZrO_2$, t-$ZrO_2$ (35), h-$Cr_2O_3$, t-$CrO_2$ |
| | 950 | 2 | m-$ZrO_2$, c-$ZrO_2$ (20 ), t-$ZrO_2$ (10 ), h-$Cr_2O_3$ |
| | 1050 | 2 | m-$ZrO_2$, h-$Cr_2O_3$ |
| 30 | 250–600 | 2–4 | c-$ZrO_2$, h-$Cr_2O_3$ |
| 30 | 800 to 1050 | 2 | Same as with $C_{Cr} = 20$ at.% |

[a] Volume fractions (%) in minority $ZrO_2$ phases as per their relative intensities in X-ray diffraction are given in the parentheses.

Table 3
Results of iodometric titration of the $ZrO_2$ sample containing 10 at.% chromium cations

| Calcining temperatures | Hot-plate (~250 °C) | 600 °C | 800 °C | 900 °C | 950 °C | 1050 °C |
|---|---|---|---|---|---|---|
| Wt.% of $Cr^{4+}$ with respect to total chromium present | 80.0 | 62.0 | 60.0 | 55.0 | 19.0 | 7.0 |
| Phases present | c | c | c | c and t | c, t and m | m |

c, t and m represent cubic, tetragonal and monoclinic phases respectively.

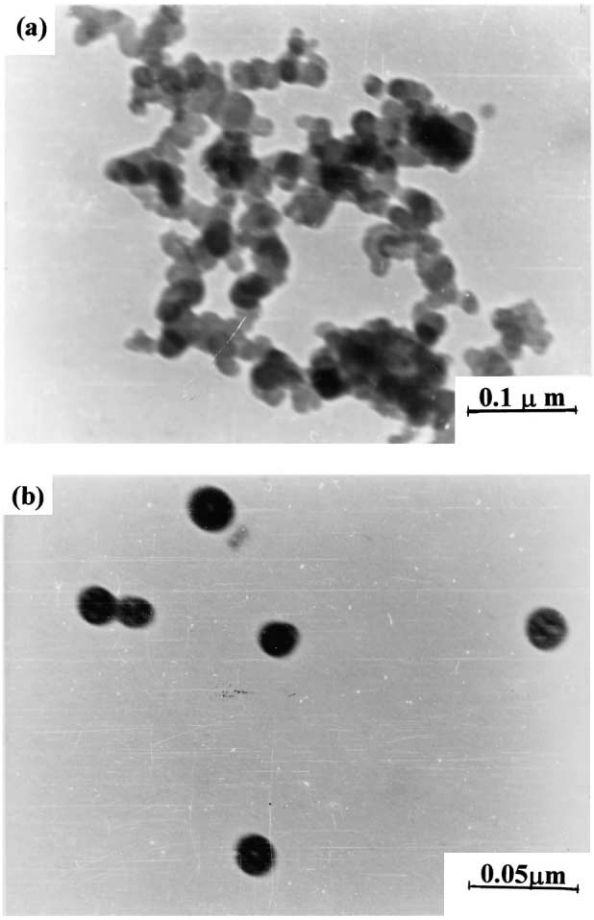


Fig. 8. TEM micrograms of stabilized c-$ZrO_2$ with $C_{Cr} = 10$ at.% on calcining the precursor at (a) 250 °C for 4 h and (b) 800 °C for 2 h.

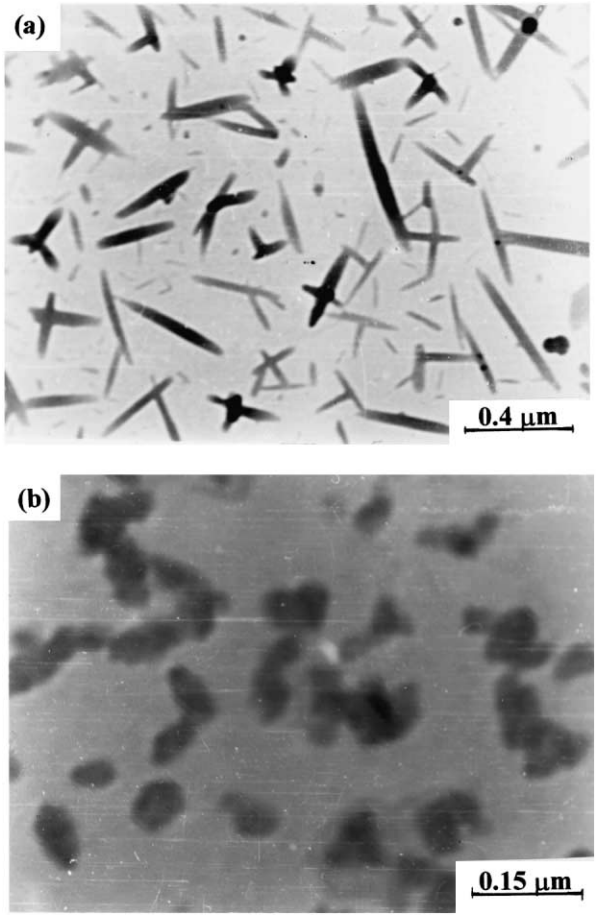


Fig. 9. TEM micrograms in (a) acicular particles of t-$ZrO_2$ and (b) oval shaped of c-$ZrO_2$ crystallized on annealing the precursor with $C_{Cr} = 10$ at.% at 900 °C for 2 h.

$$2I^- + 2Cr^{4+} \rightarrow I_2 + 2Cr^{3+}$$

$I_2$ turns into a violet color of the specimen from a light green. The acetic acid prevents $Cr^{4+}$ oxidation with air and facilitates the reaction with iodide. An intense blue color appears on adding starch. It disappears if adding sodium thiosulphate according to the following reaction.

$$2S_2O_3^{2-} + I_2 \rightarrow S_4O_6^{2-} + 2I^-$$

A blank experiment is also done without the sample, which indicates no aerial oxidation occurs to form molecular iodine. For all the samples, the above experiment is conducted to confirm the presence of $Cr^{4+}$ in all the samples. Quantitative analysis: the quantitative experiment is done by the well-known iodometric method. This experiment is done with the sample containing 10 at.% chromium. 0.2 g of calcined powder is taken in water suspension. 2.0 g K*I* is added followed by 4 ml concentrated HCl and it is kept in the dark for 15 min to complete the reaction as much as possible by dissolving the nanocrystals. The resulting solution is titrated against 0.01 N solution with the help of starch solution indicator. The result is given in Table 3.

### 3.6. Paramagnetic moments measurement

The magnetic measurement shows that the as prepared zirconia powders containing chromium ions (samples containing 10 at.%) from hot plate has the effective paramagnetic moments of 2.876 BM. This value corresponds to two unpaired electrons in $Cr^{4+}$ and also indicates the presence of very small amount of $Cr^{3+}$. The effective paramagnetic moments of the same sample calcined at 1050 °C has the value of 3.475 BM. This value is somewhat lower than the expected value indicating the presence some $Cr^{4+}$ as revealed by chemical analysis and due to antiferromagnetic interaction between chromium ions.

## 4. Conclusions

A chemical route with dispersed metal cations in a polymer of sucrose and polyvinyl alcohol is explored for synthesizing stabilized $ZrO_2$ nanoparticles with an additive of $Cr^{3+}$ and $Cr^{4+}$ in a single metastable c-$ZrO_2$ phase or in a nanocomposite with t- and/or m-phase(s).

The polymer matrix has two important functions. It acts as (i) a dispersing agents for metal ions and (ii) produces nano-structured template for generating nano particles. It dissolves metal cations in water and results in an amorphous precursor powder on evaporating the excess water over a water bath. The latter recrystallizes into a refined powder of stabilized c-$ZrO_2$ in as small as $d=5$ nm controlled crystallite size in spherical shape at as low temperature as $T_P \sim 250$ °C. It transforms to t-phase on prolonged annealing to 15 h at 900 °C. Peculiarly, t-$ZrO_2$ has an acicular shape of particles as long as 600 nm in 10–40 nm width and $\phi \leqslant 15$ aspect ratio. Clusters of particles form on small $d \sim 16$ nm crystallites in a single m-$ZrO_2$ phase at as early temperature as 1050 °C.

X-ray diffraction of stabilized c-$ZrO_2$ with $C_{cr}=5$–10 at.% $Cr^{3+}/Cr^{4+}$ at $T_P \leqslant 800$ °C show a dissolved structure of $Cr^{3+}$ and $Cr^{4+}$ in a solid solution. They do not precipitate in an independent crystalline phase at these temperatures. Chemical analysis and magnetic measurement show that the most of the chromium present in as prepared powder is $Cr^{4+}$ and as the temperature increases it transfers to $Cr^{3+}$ gradually, which drives the t–m phase transformation. In m-phase, most of the chromium is present as $Cr^{3+}$ with a small amount of $Cr^{4+}$.

## Acknowledgements

This work has been financially supported by the Indian Council for Cultural Relation (ICCR) and by the Council of Scientific and Industrial Research (CSIR), Government of India.

## References

1. Heuer, A. H., Claussen, N., Kriven, W. M. and Ruhle, M., Stability of tetragonal $ZrO_2$ particles in ceramic matrices. *J. Am. Ceram. Soc.*, 1982, **65**(12), 642–650.
2. Hannink, R. H. J., Kelly, P. M. and Muddle, B. C., Transformation toughening in zirconia containing ceramics. *J. Am. Ceram. Soc.*, 2000, **83**(3), 461–487.
3. Ishida, K., Hirota, K., Yamaguchi, O., Kume, H., Imamura, S. and Miymoto, H., Formation of zirconia solid solutions containing alumina prepared by new preparation method. *J. Am. Ceram. Soc.*, 1994, **77**(5), 1391–1395.
4. Hu, M. Z. C., Hunt, R. D., Payzant, E. A. and Hubbard, C. R., Nanocrystallization and phase transformation in monodispersed ultrafine zirconia particles from various homogeneous precipitation methods. *J. Am. Ceram. Soc.*, 1999, **82**(9), 2313–2320.
5. Xiaming, D., Qingfeng, L. and Yuying, T., Study of phase formation in spray pyrolysis of $ZrO_2$ and $ZrO_2$–$Y_2O_3$ powders. *J. Am. Ceram. Soc.*, 1993, **76**(3), 760–762.
6. Saha, S. K. and Pramanik, P., Innovative chemical method for preparation of calcia-stabilized zirconia. *Br. Ceram. Trans.*, 1995, **94**(3), 123–127.
7. Tsukada, T., Venigalla, S., Morrone, A. A. and Adair, J. H., Low temperature hydrothermal synthesis of yttrium doped zirconia powders. *J. Am. Ceram. Soc.*, 1999, **82**(5), 1169–1174.
8. Xia, B., Duan, L. and Xie, Y., $ZrO_2$ nanopowders prepared by low-temperature vapor-phase hydrolysis. *J. Am. Ceram. Soc.*, 2000, **83**(5), 1077–1080.
9. Messing, G. L., Zhang, S. C. and Jayanthi, G. V., Ceramic powder synthesis by spray pyrolysis. *J. Am. Ceram. Soc.*, 1993, **76**(11), 2707–2726.
10. Skandan, G., Hann, H., Roddy, M. and Cannon, W. R., Ultrafine-grained dense monoclinic and tetragonal zirconia. *J. Am. Ceram. Soc.*, 1994, **77**(7), 1706–1710.
11. Xie, Y., Preparation of ultrafine zirconia particles. *J. Am. Ceram. Soc.*, 1999, **82**(3), 768–770.
12. Venkatachari, K. R., Huang, D., Ostrander, S. P., Schulze, W. A. and Stangle, G. C., A combustion synthesis process for synthesizing nanocrystalline zirconia powders. *J. Mater. Res.*, 1995, **10**(3), 748–755.
13. Jayratna, M. and Yoshimura, M., Hot pressing of $Y_2O_3$-stabilized $ZrO_2$ with $Cr_2O_3$ additions. *J. Mater. Sci.*, 1986, **21**, 591–596.
14. Li, P., Chen, I. W. and Hahn, J. E. P., Effect of dopants on zirconia stabilization—an X-ray absorption study: 1. Trivalent dopants. *J. Am. Ceram. Soc.*, 1994, **77**(1), 118–128.
15. Hirano, S., Yoshinaka, M., Hirota, K. and Yamaguchi, O., Formation, characterization, and hot isostatic pressing of $Cr_2O_3$ doped $ZrO_2$ (0.3 mol%) $Y_2O_3$ prepared by hydrazine method. *J. Am. Ceram. Soc.*, 1996, **79**(1), 171–176.
16. Stefanic, G., Popovic, S. and Music, S., Influence of $Cr_2O_3$ on the stability of low temperature t-$ZrO_2$. *Mater. Lett.*, 1998, **36**, 240–244.
17. Minh, N. Q., Ceramic fuel cells. *J. Am. Ceram. Soc.*, 1993, **76** (3), 563–588.
18. Wen-Xiang, W, Zheng, L. and Fan, L., Study of the internal action and existent state of $ZrO_2$ in fused iron catalysts of different compositions. *J. Solid State Chem.*, 1993, **107**, 201–210.
19. Garvie, R. C., Hannink, R. H. and Pascoe, R. T., Ceramic Steel?. *Nature*, 1975, **258**, 703–704.
20. Ray, J. C., Pramanik, P. and Ram, S., Formation of $Cr^{3+}$ stabilized $ZrO_2$ nanocrystals in a single cubic metastable phase by a novel chemical route using sucrose and polyvinyl alcohol matrix. *Mater. Lett.*, 2001, **48**(15), 281–291.
21. Ray, J. C., Pati, R. K. and Pramanik, P., Chemical synthesis and structural characterization of nanocrystalline powers of pure zirconia and yttria-stabilized zirconia (YSZ). *J. Eur. Ceram. Soc.*, 2000, **20**, 1289–1295.
22. Pathak, A. and Pramanik, P., In *Nano Particles of Oxides through Chemical Methods, Nanomaterials*, ed. D. Chakravorty. Indian National Science Academy, New Delhi, 2001.
23. Klug, M. P. and Alexander, L. E., *X-ray Diffraction Procedure for Polycrystalline and Amorphous Materials*. Wiley, New York, 1974 (pp. 634).
24. X-ray Powder Diffraction, JCPDS File (a) 6-0504, h-$Cr_2O_3$, (b) 13-307, m-$ZrO_2$, (c) 9-0332, t-$CrO_2$, (d) 27-.997, c-$ZrO_2$, and (e) 24-1164, t-$ZrO_2$.
25. Toraya, H., Yoshimura, M. and Somiya, S., Quantitative analysis of monoclinic-stabilized cubic zirconia system by X-ray diffraction. *J. Am. Ceram. Soc.*, 1984, **67**(9), C183–184.